Journal of Marine Science and Technology

Volume 31 | Issue 4 Article 18

Cooling Performance Analysis for Mobile Vehicles by Thermal Resistance Network

Chia-an Yang
Department of Marine Engineering(DME), National Taiwan Ocean University(NTOU), Keelung 202301, Taiwan

Jung-Chang Wang
Department of Marine Engineering(DME), National Taiwan Ocean University(NTOU), Keelung 202301, Taiwan

Pi-Hsia Yen
Department of Tourism and Leisure Management, Yu Da University of Science and Technology, Miaoli County, 36143, Taiwan, R.O.C., phyen@ydu.edu.tw

Recommended Citation

Yang, Chia-an; Wang, Jung-Chang; and Yen, Pi-Hsia (2023) "Cooling Performance Analysis for Mobile Vehicles by Thermal Resistance Network," *Journal of Marine Science and Technology*: Vol. 31: Iss. 4, Article 18.
DOI: 10.51400/2709-6998.2723
Available at: https://jmstt.ntou.edu.tw/journal/vol31/iss4/18

RESEARCH ARTICLE

Cooling Performance Analysis for Mobile Vehicles by Thermal Resistance Network

Chia-An Yang [a], Pi-Hsia Yen [b,*], Jung-Chang Wang [a,**]

[a] Department of Marine Engineering(DME), National Taiwan Ocean University(NTOU), Keelung, 202301, Taiwan
[b] Department of Tourism and Leisure Management, Yu Da University of Science and Technology, Miaoli County, 36143, Taiwan, ROC

Abstract

This paper used CFD software to simulate the cooling situation of the engine space of a mobile vehicle. In particular, we used a thermal resistance network diagram to calculate the heat flux at each position of the power system. The CFD simulation results are discussed in Section 3 of this paper: the error between the simulation results and the experiment was 10.07 %. Noteworthily, the thermal resistance network diagram proposed in this paper can reduce the time for numerical simulation by evaluating the heat flux at each position of the power system.

Key words: Heat dissipation, Heat transfer parameters, Armored car

1. Introduction

In this study, we investigated the cooling performance of a powertrain room in a four-stroke, six-cylinder diesel engine vehicle. The analysis encompassed the engine, gearbox, and turbocharger, as well as other subsystems such as the cooling system, intake and exhaust system, AC generator, air compressor, power steering pump, hydraulic pump, and brake system. The entire powertrain system was electronically controlled, with the electronic control unit (ECU) partitioning and managing the system behavior through real-time sensing and feedback signals from the engine and gearbox. It must be noted, however, that the high loads imposed on the powertrain system during mobile operations can result in higher temperatures in the powertrain room. In addition, inadequate cooling system performance may lead to failures in electronic systems such as the ECU.

Based on the existing cooling system design, we measured the surface temperatures of the powertrain components, analyzed their potential impact, and integrated experimental and simulation analysis techniques to establish the powertrain system's numerical simulation model of the powertrain system. Furthermore, we employed Newton's cooling law and thermal resistance analysis to express the relationship between cooling performance and power room heat source distribution.

Murakami and Kato [1] used the k-ε model to simulate the interior flow field situation. Meanwhile, Han [2] extended this application to cars and analyzed the heat transfer distribution. The simulation parameters were set through experimental values, including the air outlet temperature. The vehicle was set to two conditions, namely the isothermal boundary and adiabatic wall. The results showed that the conditions of the isothermal boundary are more consistent than the adiabatic wall. The research involving mobile states and numerical simulation processes needed to consider the aerodynamics of the vehicle's external airflow to match the pressure and velocity distribution in the real operational flow field.

Related research discussed numerical simulations of vehicle aerodynamic resistance. For instance,

Received 3 May 2023; revised 10 November 2023; accepted 13 November 2023.
Available online 15 December 2023

* Corresponding author.

** Corresponding author.
E-mail addresses: phyen@ydu.edu.tw (P.-H. Yen), jcwang@ntou.edu.tw (J.-C. Wang).

https://doi.org/10.51400/2709-6998.2723

Makowski [3] used Fluent to perform modifications on the intake of the F-1 race car's inlet-air box, with the calculation domain including the inlet-air box and its surrounding areas and using a hybrid mesh with 1.04 million cells. Kleber [4] also used Fluent to simulate the external flow field of a sedan, with approximately 3 million hybrid mesh in the numerical simulation process. In accelerating convergence, a first-order upwind scheme was used for the first 300 iterations of the simulation process, followed by a second-order upwind scheme for further iterations. The error between the estimated drag coefficient and experimental values was approximately 5−10 %. Current simulations of vehicle aerodynamics use steady-state and incompressible flows. The accuracy of simulation results was highly dependent on the quality of the mesh, usually compared with experimental data.

The results and discussions of the cooling performance analysis can be presented not only by temperature but also through the Nusselt number, equivalent heat transfer coefficient, thermal resistance, and other methods [5−7]. Olsson et al. [8] used computational fluid dynamics (CFD) to investigate the heat transfer phenomenon of a cylinder placed in a semi-enclosed area and subjected to impinging airflow. Noteworthily, the SST (Shear Stress Transport) model in CFX 5.5 with k-ε, k-ω and SST modes provided the most accurate prediction. The local Nusselt number was used to represent the heat transfer effectiveness at different locations, and the correlation between the Nusselt number and factors − such as Reynolds number (23000−100000) around the cylinder, distance from the jet inlet to the cylinder, ratio of the distance from the jet inlet to the cylinder diameter, and cylinder curvature − was discussed. The results showed that the local Nusselt number varied with the surface position of the cylinder but was less influenced by the distance from the jet flow to the cylinder.

Yang et al. [9] conducted a study on the influence of a nozzle angle on the cooling effectiveness of an aluminum plate during the aluminum plate processing cooling process. The cooling target was a 300 mm × 10 mm aluminum alloy flat plate with a nozzle diameter of 2 mm. The distance between the flat plate and the nozzle was 150 mm, and the spray angle ranged from 10° to 110°. In addition, the simulation process used the SIMPLE algorithm. The results were discussed based on the average surface temperature and heat transfer coefficient. The results showed that larger spray angles resulted in a more uniform average surface temperature, thus improving the uniformity of the cooling process. The optimal range of spray angles for cooling was found to be 70°−90°. At a spray angle of 70°, the average heat transfer coefficient reached approximately 280 W/m^{2}Kl, and the average temperature of the aluminum plate dropped to 685 °C.

Li et al. [10] conducted a study on the heat dissipation effectiveness of plate-fin heat sinks. They investigated parameters, including Reynolds number (5000−25000), the distance ratio between the inlet and the fin to the nozzle diameter (Y/D), ranging from 4 to 28, the ratio of the single fin width to overall fin length (W/L) ranging from 0.08125 to 0.15625, and the ratio of the single fin height to the overall fin length (H/L), ranging from 0.375 to 0.625. The results were discussed based on thermal resistance. In particular, the findings showed that increasing the Reynolds number reduced thermal resistance and improved cooling effectiveness. The appropriate distance between the nozzle and the fin also reduced the thermal resistance. Additionally, the height of the fin had a more significant impact on the thermal resistance compared to the width. Through thermal resistance analysis, the Reynolds number of 20000, Y/D of 16, W/L of 0.1375, and H/L of 0.625 were found to be the optimal parameters for the lowest thermal resistance and the best cooling effectiveness. Notably, the heat dissipation effectiveness discussed in thermal resistance analyses has been applied in various fields.

2. Research methods

2.1. Experimental program

The vehicle dimensions are shown in Fig. 1, with the powertrain system located in the front of the vehicle, serving as the heat source in the engine room. The vehicle had two air intakes and one exhaust outlet for dissipating heat from the engine room, which included two radiator fans to remove the heat. It must be noted that the thermal performance experiments in this study were conducted under mobile operation. Therefore, the experimental process involved increasing the vehicle load by driving on an uphill road segment, followed by driving on a flat road segment and repeating the uphill process about 15 times. The total testing time was 30 min, with the air conditioning system turned off during the experiments. In addition, the experiment was briefly paused twice during the process, with an ambient temperature of 16 °C. The heat generated by the engine after starting was dissipated by the incoming air into the engine room. The temperatures were measured using thermocouples and infrared thermography, while the wind speed was measured using the TES hot-wire anemometer.

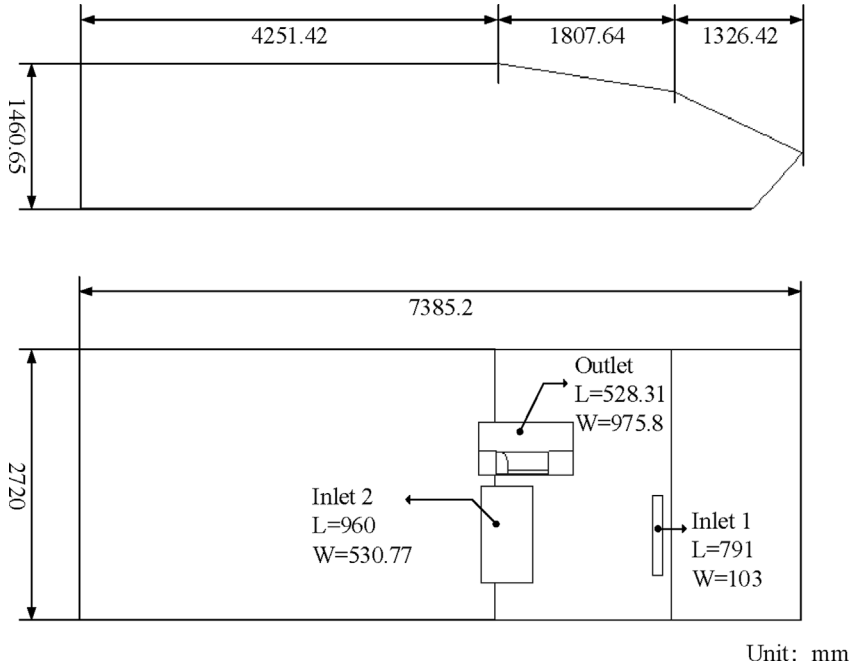

Fig. 1. Vehicle dimensions.

The schematic diagram of the experimental setup is shown in Fig. 2.

During the mobile testing process, the vehicle was driven on a flat road at approximately 20 km/hr, with an external wind speed ranging from 4.6 m/s to 6.5 m/s. The temperatures were measured at eight positions, including inlet 1, inlet 2, outlet, engine surface, charge cooler's inlet, charge cooler's outlet, radiator's inlet, and radiator's outlet, as shown in Fig. 3.

It can be observed in this study that the outlet temperature from the engine room immediately dropped to about 15 °C, as shown in Fig. 3(a). On the other hand, the charge cooler's inlet temperature was directly related to the exhaust temperature decreasing around 40 °C, as shown in Fig. 3(b).

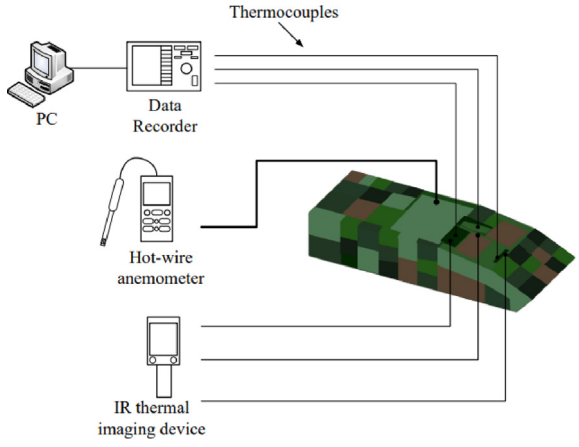

Fig. 2. Schematic diagram of the experimental setup.

These results are due to the brief pause during the process. Thus, the cylinder's internal temperature was less affected by the ambient temperature, resulting in the water cooler's inlet temperature remaining relatively stable, as shown in Fig. 3(c). The inlet temperature of the water cooler could be used to determine the engine experiences at a maximum thermal load condition during the entire mobile experiment. Through this mobile testing process, the heat dissipation capability and characteristics of the powertrain system under a maximum thermal load during driving conditions were obtained, as shown in Fig. 4.

Under mobile operation, the cooling air entered the powertrain room through inlet 1 and inlet 2. Subsequently, it was exhausted from the powertrain room by a fan, with an exhaust temperature of 75.9 °C. The cooling air inside the powertrain room cooled the engine, turbocharger, air cooler, and water cooler. Consequently, the surface temperature of the engine was 88.7 °C while that of the turbocharger was 190.8 °C.

2.2. Numerical simulation

Numerical analysis is a field of CFD that integrates fluid mechanics, discrete mathematics, numerical methods, and computer technology. It can be used after experiments to conduct more comprehensive flow field analysis by adjusting parameters and discuss experimental scenarios under different simulation parameter settings.

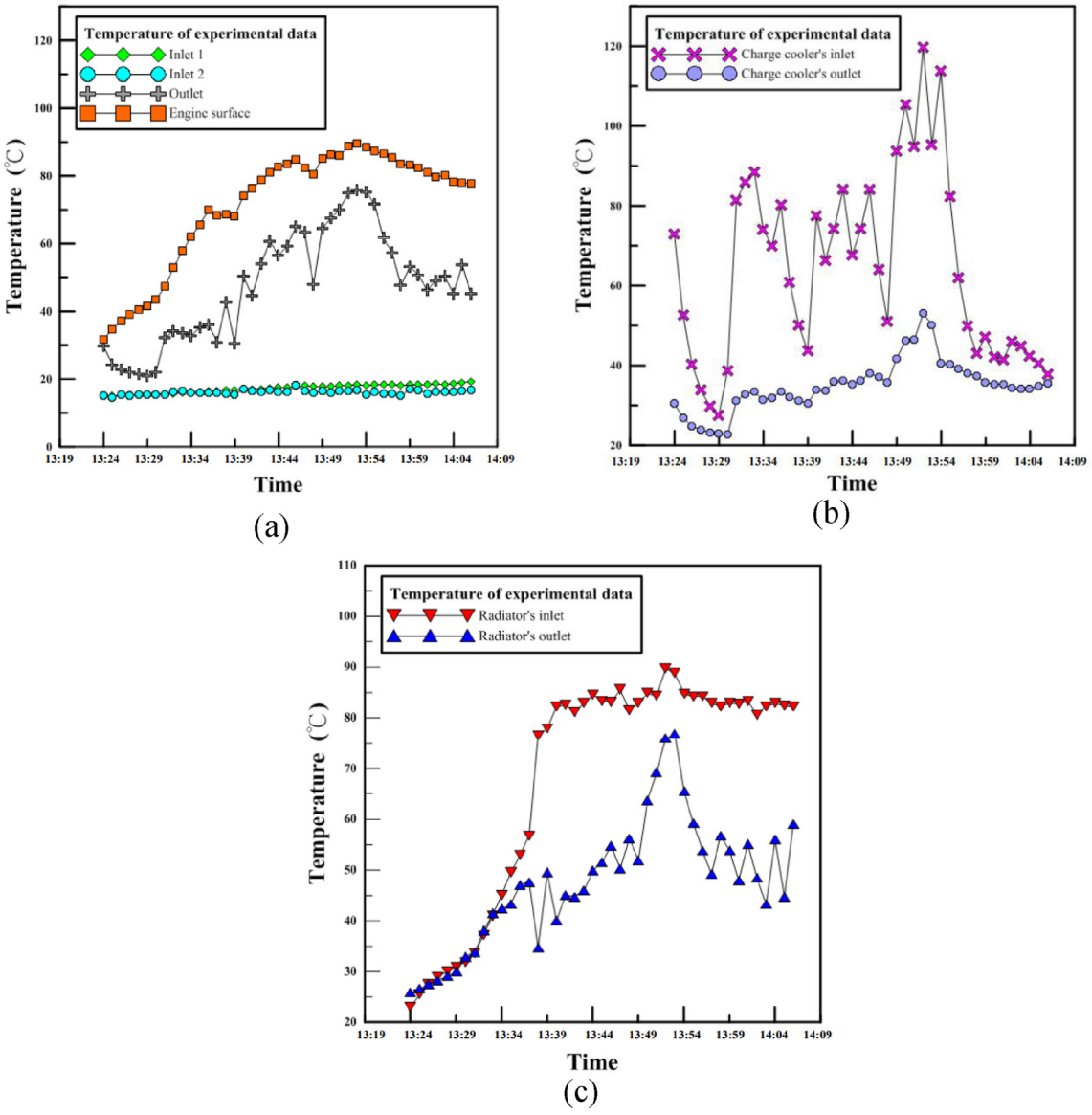

Fig. 3. (a) Temperature during the experiment. (b) Temperature during the experiment. (c) Temperature during the experiment.

This study used ANSYS ICEPAK for analysis and to simplify the vehicle body and powertrain components into a simulation model, as shown in Fig. 5. The model includes several block-shaped heat sources, such as the engine, turbocharger, gearbox, water cooler, and air cooler.

The mobile operation simulation used the zero-equation model for turbulent flow analysis. The meshes were approximately 3.62 million. The boundary conditions are as follows:

1. The working fluid was assumed to be incompressible.
2. The ambient temperature was 16 °C.
3. The flow condition was turbulent, with gravity acting in the negative y-direction.
4. Radiative heat effects were neglected.
5. The mobile motion process was approximated by a maximum wind speed of −4.9 m/s in the x-direction.

During the operation process, the engine drove the propulsion bearing as energy passed through several mechanical structures, causing wear losses. This part of the loss was simplified at a gearbox position in the simulation process. In particular, the fan speed was 2200 rpm, the volume flow was 2.64 m^3/s, and the fan static pressure was 759.611 N/m^2. The fuel oil consumption was 11.594 L, the oil density was 0.8 kg/m^3, and the heating value was 11,025 kcal/kg.

The thermal energy provided by fuel oil was 237.787 (kW), calculated using Eq (1).

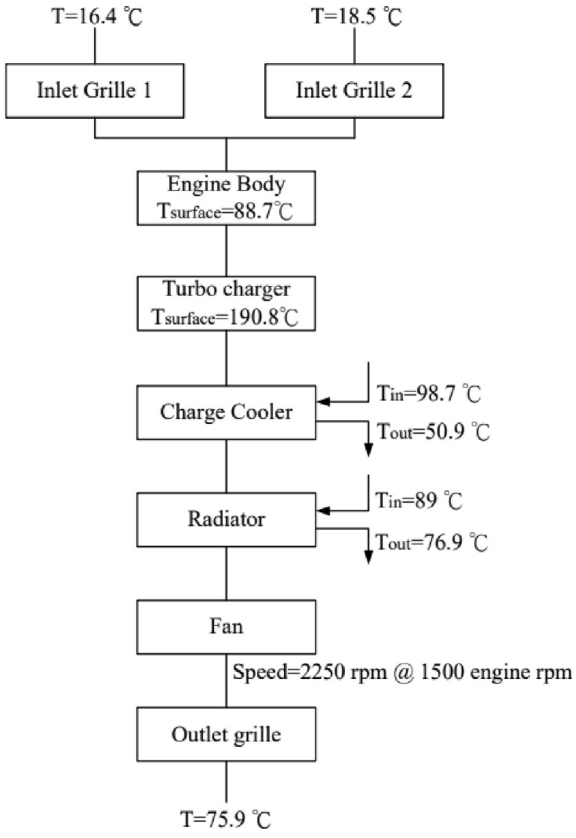

Fig. 4. Heat dissipation capability and characteristics of the powertrain system.

$$Q_{in} = consumption \times heating\ value \times (1 - Engine\ heat\ efficiency - 2.0\%) \quad (1)$$

In Eq (1), 2.0% represents the losses from incomplete combustion. The engine heat efficiency was around 34 %. The remaining energy is lost through friction, exhaust, and heat consumption. The heat transfer loss should be 147.666 (kW).

2.3. Thermal resistance analysis

The thermal performance's experimental environment was limited. Hence, this study proposed a thermal resistance network diagram to analyze the heat dissipation of each power system heat source (i.e., engine, turbocharger, gearbox, water cooler, and air cooler) as a setting parameter for the simulation. Thermal resistance is defined by Eq (2).

$$R_{thermal} \equiv \frac{\Delta T}{Q} \quad (2)$$

where $R_{thermal}$ represents the thermal resistance (°C/W), ΔT is the temperature difference (°C), and Q is the heating power (Watt).

Based on the definition, thermal resistance can be used to evaluate the heat dissipation performance of a heat sink. A larger thermal resistance indicates that heat transfer is less efficient, resulting in a higher temperature of the heat source for the same heating power. Conversely, a smaller thermal resistance results in a lower temperature of the heat source and a better heat dissipation performance. Therefore, this study proposed a thermal resistance network during mobile operation, as shown in Fig. 6.

As shown in Fig. 6, the total heat energy generated by the engine is referred to as Q_{in}, which is divided into three parts transferred out of the engine. The first part is Q_1, the heat energy carried away by the exhaust. The second part is Q_2, the heat energy carried away by the cooling water, and the third part is Q_8, the heat energy transferred to the bearing through the crankshaft. Among them, the heat energy of Q_1 is divided into three parts after passing through the turbocharger: Q_3 is the heat energy discharged to the atmosphere through the exhaust pipe; Q_4 is the heat energy transferred to the surface of the turbocharger; Q_5 is the heat energy transferred to the intake side of the turbocharger. Further, the energy of Q_2 is divided into two parts: Q_6 is transferred through the jacket cooling water, while Q_7 is transferred through the cylinder's cover to the surface of the engine.

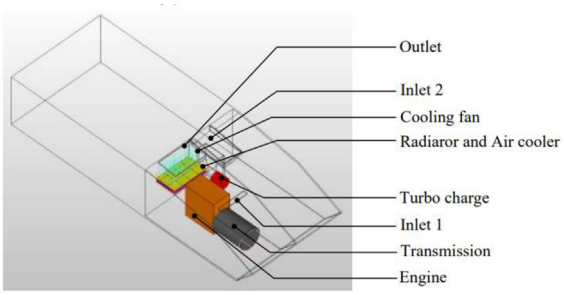

Fig. 5. Simulation model.

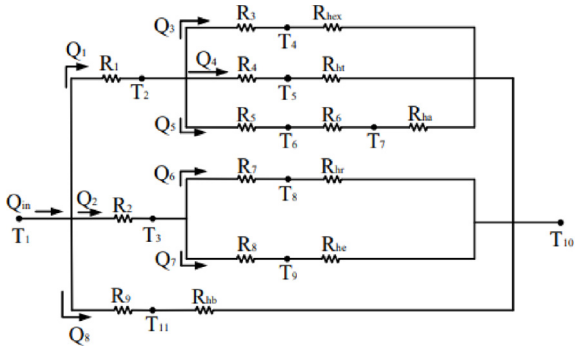

Fig. 6. Thermal resistance network for powertrain system during mobile operation.

The temperature values are defined as follows:
T_1 is the average temperature inside the engine;
T_2 is the exhaust temperature of the engine;
T_3 is the inlet temperature of the water cooler;
T_4 is the exhaust outlet temperature of the engine;
T_5 is the temperature of the turbocharger;
T_6 is the inlet temperature of the intake cooler;
T_7 is the outlet temperature of the intake cooler;
T_8 is the outlet temperature of the water cooler;
T_9 is the surface temperature of the engine;
T_{10} is the ambient temperature;
T_{11} is the surface temperature of the bearing.
The thermal resistances are defined as follows:
R_1 is the resistance between the engine and the turbine;
R_2 is the resistance between the engine and the cooling water outlet;
R_9 is the resistance made by friction;
R_3 is the resistance between the turbine and the exhaust end;
R_4 is the resistance between the turbine bearing and turbine surface;
R_5 is the resistance between the turbine bearing and compressor wheel;
R_6 is the resistance between the compressor wheel and the turbocharge air inlet;
R_7 is the resistance between the cooling water inlet and outlet;
R_8 is the resistance between the cooling water and the engine surface;
R_{hex} is the resistance between the exhaust end and ambient temperature;
R_{ht} is the resistance between the turbine surface and ambient temperature;
R_{ha} is the resistance between the turbocharge air inlet and ambient temperature;
R_{hr} is the resistance between the cooling water outlet and ambient temperature;
R_{he} is the resistance between the engine surface and ambient temperature;
R_{hb} is the resistance between the engine shaft surface and ambient temperature.

Exhaust gas usually contains 20−45 % fuel oil thermal energy in the diesel engine. On the other hand, cooling water usually contains 10−30 %, and lubricating oil contains 5−15 % fuel oil thermal energy [11−13]. In this study, the piston was derived after burning and transmitting to the gearbox through the connecting shaft and crankshaft. Then, wear occurred when power was transmitted. While diesel engine friction losses were generally considered 10 %, this part of energy was taken into other parts like cooling water and lubricating oil. Hence, we removed the repeated heat calculation under mobile operation. The turbocharge air-carried thermal energy was calculated using Eq (3).

$$Q_5 = \dot{m}_{air\ flow} \times C_p \times (T_6 - T_{10}) \tag{3}$$

where $\dot{m}_{air\ flow}$ represents the inlet quality of combustion air(kg), which is 0.47 kg/s when 2200 rpm. C_P is the specific heat of the gas at constant pressure.

The heat transfer model of the diesel engine combustion chamber is displayed in Fig. 7. T_g represents the combustion gas temperature in the cylinder, while h_g represents its convection coefficient. T_c is the cooling water temperature, with h_c as its convection coefficient. Because it could be treated as a constant, the heat transfer process of the cylinder wall was a periodic change and regarded as a steady state [14,15]. The engine surface's lost thermal energy was calculated using Eq (4).

$$Q_7 = k \times A \times \frac{\Delta T}{t} = \frac{T_3 - T_9}{R_8} \tag{4}$$

Considering the complexity of the mechanical structure of the engine, we treated it as a rectangular parallelepiped to calculate its theoretical resistance (Fig. 8).

Fig. 9 shows organized existing information on the thermal resistance network, indicating the experimental data and previous research as the red points and orange arrows, respectively.

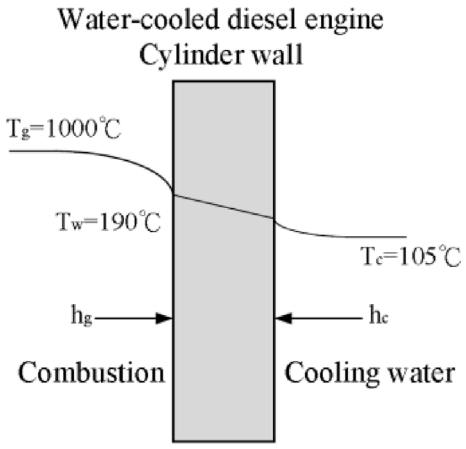

Fig. 7. Heat transfer model of the diesel engine combustion chamber.

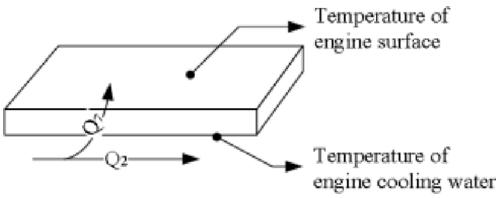

Fig. 8. Simplified diagram of heat transfer on engine surface.

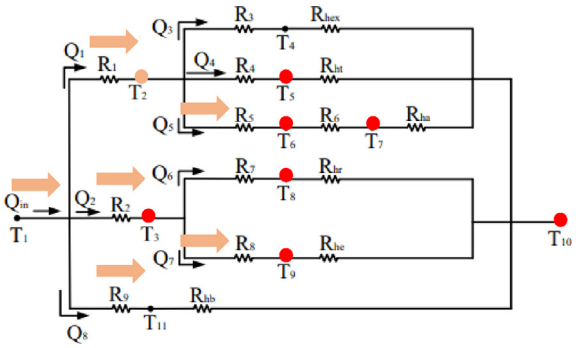

Fig. 9. Organized existing information on the thermal resistance network.

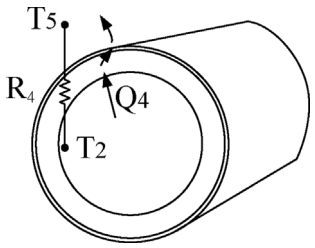

Fig. 10. Simplified diagram of the heat transfer on the turbine.

Based on Fig. 9, we only had to calculate the theoretical resistance of R_4 to find Q_4 and evaluate heat Q_2 and Q_9 to determine the model parameters. R_4 is the resistance between the turbine bearing and the turbine surface, simplified into a cylinder, as shown in Fig. 10. The resistance is calculated using Eq (5).

$$R_4 = \frac{\ln\left(\frac{r_2}{r_1}\right)}{2\pi k_1 L} + \frac{\ln\left(\frac{r_3}{r_2}\right)}{2\pi k_2 L} = \frac{T_2 - T_5}{Q_4} \tag{5}$$

The turbine was simplified as a cylinder with an outer diameter of r_2 and an inner diameter of r_1. The shell was wrapped with an insulation cotton, with an outer diameter of r_3. L refers to the length, k_1 refers to the heat transfer coefficient of the turbine shell material (used 12.5 W/m · K), and k_2 refers to the heat transfer coefficient of the insulation cotton (used 0.174 W/m · K).

3. Results and discussion

The simulated result of the speed and temperature distribution in the z-direction are shown in Fig. 11. The simulation found that the simulated wind speed at the measurement location was

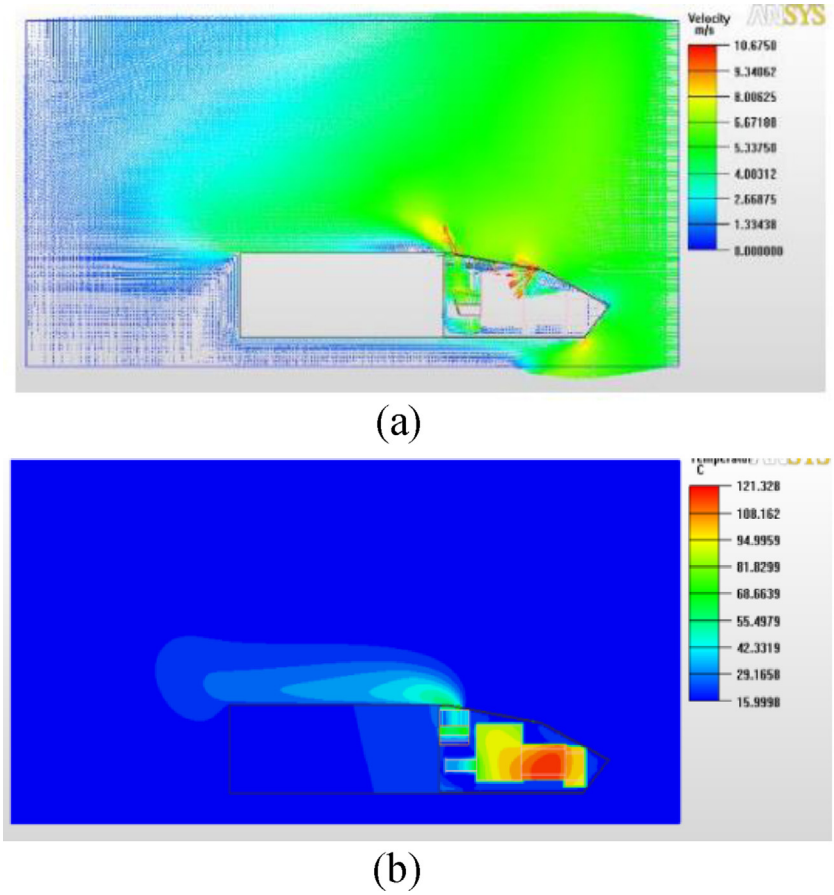

Fig. 11. (a) Speed distribution(z-direction). (b) Temperature distribution(z-direction).

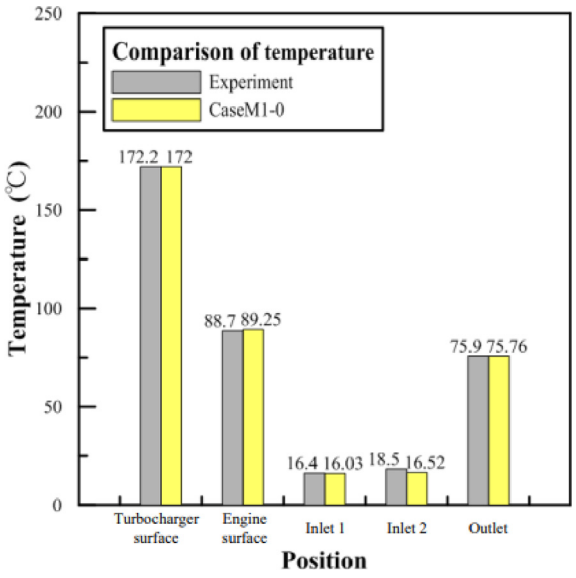

Fig. 12. Comparison between experimental and simulated results.

5.89 m/s, within the range of experimental wind speeds. The comparison between the mobile experimental and simulated results for the temperature at the same measurement location is shown in Fig. 12. Noteworthily, the largest temperature error was 1.98 °C at inlet 1. This discrepancy is likely caused by the simplification process of the model.

The numerical simulation results of the study are discussed according to the temperature and the heat transfer coefficient. The heat transfer coefficient was calculated using Newton's law of cooling. Its valve was 88.190 W/m^{2}K.

4. Conclusion

(1) This study simplified the simulation process, considering only the following heat sources: engine, turbocharger, gearbox, air cooler, and water cooler. The error between the simulation and the experiment was 10.7 %.

(2) The simulation model established in this study can be used as a reference for the cooling performance of derivative vehicle models in subsequent development. In particular, this model can help reduce research costs.

(3) Based on the fitted model obtained from the mobile experiments, the average heat transfer coefficient inside the powertrain system was 88.190 W/m^{2}K.

(4) The thermal resistance network diagram proposed in the study can be used for future analyses of similar vehicle power rooms.

Declaration of competing interest

The authors declare that they have no known competing financial interests or personal relationships that could have appeared to influence the work reported in this paper.

References

[1] Murakami S, Kato S. Numerical and experimental study on room airflow 3D predictions using the k-ϵ turbulence model. Build Environ 1989;24(1):85−97.
[2] Han T. Three-dimensional navier-stokes simulation for passenger compartment cooling. Int J Vehicle Des 1989;10(2): 175−86.
[3] Makowski Francis T. Computer simulation helpsengineers improve ferrari formula one aerodynamics," the high technology cars and engines symposium. Italy: Mostra-Convegno; 2001.
[4] Kleber A. Simulation of air flow around an OPEL ASTRA vehicle with FLUENT. J Articl FluentSoft Users 2001;JA132: 1−6.
[5] Chen Wei-Jui. Experimental analysis of thermal performance of embedded heat pipes heat sink and predict the performance curves of U-type and L-type heat pipes (Master's thesis). Keelung: National Taiwan Ocean University; 2012.
[6] Liou Guan-Cing. Heat Transfer and Illumination Analysis of Heat Conductive Substrate and Optimal Design of Matrix Array fins for High Power LED Lamp (Master's thesis). Keelung: National Taiwan Ocean University; 2014.
[7] Yu Fu-Hsiung. 3-D Structure Design and Thermal Performance Analysis of Non-metallic LED Bulb (Master's thesis). Keelung: National Taiwan Ocean University; 2014.
[8] M Olsson EE, M Ahrné L, C Trägårdh A. Heat transfer from a slot air jet impinging on a circular cylinder. J Food Eng 2004; 63(4):393−401.
[9] Yang Haibo, Cao Xinchun, Sun Xuewen. Effects of Spray Angle on Spray Cooling of Extruded Aluminum Alloy Plate. In: AASRI conference on modeling. Identification and Control, Chair American Applied Sciences Research Institute, USA; 2012. p. 630−5.
[10] Li Hung-Yi, Chen Kuan-Ying. Thermal performance of plate-fin heat sinks under confined impinging jet conditions. Int J Heat Mass Tran 2007;50:1963−70.
[11] Kang Hyungmook, Ahn Hyunchul, Min Kyoungdoug. Smart cooling system of the double loop coolant structure with engine thermal management modeling. Appl Therm Eng 2015;79:124−31.
[12] Pulkrabek Willard W. Engineering Fundamentals of the Internal Combustion Engine. Prentice-Hall, Englewood Cliffs NJ; 2004.
[13] Miyairi Y. Soc Automot Eng 1989;880187.
[14] Ferguson CR. Internal Combustion Engine. New York: Wiley; 1986.
[15] Heywood JB. Internal Combustion Engine Fundamentals. In: International cd. New York: McGraw-Hill; 1998.